The trajectory of slender curved liquid jets for small Rossby number

Alsharif, Abdullah Madhi; Decent, Stephen P; Părău, Emilian I; Simmons, Mark J H; Uddin, Jamal

DOI:
10.1093/imamat/hxy054

Document Version
Peer reviewed version

Citation for published version (Harvard):
Alsharif, AM, Decent, SP, Părău, EI, Simmons, MJH & Uddin, J 2019, 'The trajectory of slender curved liquid jets for small Rossby number', *IMA Journal of Applied Mathematics*, vol. 84, no. 1, pp. 96-117. https://doi.org/10.1093/imamat/hxy054

IMA Journal of Applied Mathematics (2018) Page 1 of 21
doi:10.1093/imamat/xxx000

The trajectory of slender curved liquid jets for small Rossby number

ABDULLAH MADHI ALSHARIF
Department of Mathematics and Statistics, Taif University, Al Hawiah, P. O. Box 888, P. Code 21974, Saudi Arabia

STEPHEN P. DECENT*
Department of Mathematics and Statistics, Lancaster University, Lancaster LA1 4YF, UK
*Corresponding author: s.decent@lancaster.ac.uk

EMILIAN I. PĂRĂU
School of Mathematics, University of East Anglia, Norwich NR4 7TJ, UK

MARK J. H. SIMMONS
School of Chemical Engineering, University of Birmingham, Birmingham B15 2TT, UK

AND

JAMAL UDDIN
School of Mathematics, University of Birmingham, Birmingham B15 2TT, UK

[Received on 13 August 2018]

Wallwork *et al.* (2002) and Decent *et al.* (2002) developed an asymptotic method for describing the trajectory and instability of slender curved liquid jets. Decent *et al.* (2018) showed that this method is accurate for slender curved jets when the torsion of the centreline of the jet is small or $O(1)$, but the asymptotic method may become invalid when the torsion is asymptotically large. This paper examines the torsion for a slender steady curved jet which emerges from an orifice on the outer surface of a rapidly rotating container. The torsion may become asymptotically large close to the orifice when the Rossby number $Rb \ll 1$, which corresponds to especially high rotation rates. This paper examines this asymptotic limit in different scenarios and shows that the torsion may become asymptotically large inside a small inner region close to the orifice where the jet is not slender. Outer region equations which describe the slender jet are determined and the torsion is found not to be asymptotically large in the outer region, and these equations can always be used to describe the jet even when the torsion is asymptotically large close to the orifice. It is in this outer region where travelling waves propagate down the jet and cause it to rupture, and so the method developed by Wallwork *et al.* (2002) and Decent *et al.* (2002) can be used to study the jet dynamics even when the torsion is asymptotically large at the orifice.

Keywords: Liquid jets, surface tension, rotation.

1. Introduction

A method was developed by Wallwork *et al.* (2002) and Decent *et al.* (2002) to study slender curved liquid jets that emerge from an orifice on the outer surface of a rapidly rotating cylindrical container where the axis of rotation of the cylinder is vertical. Decent *et al.* (2002) included gravity, while Wallwork *et al.* (2002) neglected gravity in the model. In those papers, the trajectory of the curved jet was determined under steady conditions and then perturbed with small linear unstable travelling waves that propagate down the jet and cause it to rupture. This method was extended in a series of papers such

as by Parau *et al.* (2006, 2007) and Uddin *et al.* (2006, 2008) to examine nonlinear effects and other physical effects such as non-Newtonian viscosity and surfactants. The results of these computational studies were compared successfully to laboratory experiments by Wallwork *et al.* (2002), Wong *et al.* (2004), Partridge *et al.* (2005) and Hawkins *et al.* (2010). This work was motivated by industrial manufacturing processes called prilling (Wallwork *et al.* 2002) based around droplet production. Other related papers include the examination of a viscous Cosserat model (Arne *et al.* 2010), particle laden viscous jets (Gramlich & Piesche 2012), viscoelastic jets (Marheineke *et al.* 2016), curved viscous fibres (Marheineke & Wegener 2009, Panda *et al.* 2008)), the effect of crossflow (Ng *et al.* 2008), nanofibre formation (Noroozi *et al.* 2017), polymeric fluids (Riahi 2017) and coiling jets (Ribe 2004, Ribe *et al.* 2006), which illustrate the wide range of applications for curved jets and together demonstrate the rich and varied dynamics that can result from these complex curved flows.

Wallwork *et al.* (2002) and Decent *et al.* (2002) used a coordinate system that is locally cylindrically polar on a short lengthscale, but which curves on a longer lengthscale, to derive the various equations that describe the steady slender jet and unsteady jet dynamics, and used the method of multiple scales to describe the jet using a small parameter $\varepsilon \to 0$, where $\varepsilon = a/s_0$, a is the radius of the orifice from which the jet emerges and s_0 is the radius of the rotating cylindrical container. Shikhmurzaev & Sisoev (2017) showed that the torsion of the centreline of a jet, denoted here by κ_2, can influence the flow of the jet, and also produced equations that describe a curved jet which are valid even when the jet is not asymptotically slender by using differential geometry. Following that paper, Decent *et al.* (2018) showed that the method used by Wallwork *et al.* (2002) and Decent *et al.* (2002) is accurate for slender jets when the torsion is small or $O(1)$, and also showed that the methods developed by Wallwork *et al.* (2002), Decent *et al.* (2002) and Shikhmurzaev & Sisoev (2017) produce jet equations that agree at leading-order in ε. Decent *et al.* (2018) also showed that their slender jet model may break-down if the torsion is asymptotically large, and in particular argued that this may occur if $\kappa_2 = O\left(\varepsilon^{-1}\right)$ or larger. This asymptotically large torsion corresponds to the basis vectors of the coordinate system no longer being orthogonal and this non-orthogonality having an effect at leading-order on the jet, based upon asymptotic expansions using ε (see Decent *et al.* 2018): in other words, the coordinate system used by Wallwork *et al.* (2002) and Decent *et al.* (2002) may become inappropriate to describe the jet effectively when κ_2 is sufficiently asymptotically large. However, in all previous situations examined numerically or in laboratory experiments, the torsion has been small (and often zero) or at most $O(1)$ (e.g. Wallwork *et al.* 2002, Decent *et al.* 2002, Wong *et al.* 2004, Partridge *et al.* 2005, Parau *et al.* 2006, 2007, Uddin *et al.* 2006, 2008 and Hawkins *et al.* 2010), and so a situation where the torsion may become large has not previously been examined in any detail.

This paper concentrates on steady solutions to the slender jet equations which describe the jet's curved trajectory. The steady jet equations derived by Decent *et al.* (2002) are shown below in equations (1.1). The coordinate of the following ordinary differential equations is the arclength s along the centreline of the curved liquid jet, measured from the orifice which is located at $s = 0$, so that $s \geqslant 0$ along the jet. The arclength s is nondimensionalised with respect to s_0. In the following equations $u_0(s)$ is the leading-order speed of the jet, $R_0(s)$ is the local radius of the jet measured away from the jet's centreline (i.e. the location of the free-surface of the jet which marks the boundary between the liquid and the surrounding air), and $X(s)$, $Y(s)$ and $Z(s)$ give the location of the steady centreline of the curved liquid jet relative to Cartesian coordinates x, y, z, where this Cartesian coordinate system rotates with the rotating cylinder. The y-axis points vertically upwards. The x-axis points away from the axis of the rotating cylindrical container and through the centre of the orifice so that the x-axis is normal to the surface of the rotating container. The z-axis is tangential to the surface of the rotating cylindrical container. The origin of the x, y, z coordinate system is located at the centre of the orifice where the jet

emerges from the rotating container. Therefore the centreline of the jet is the curve $x = X(s)$, $y = Y(s)$ and $z = Z(s)$. The rotating cylinder, the path of the jet and the coordinate system are sketched in Figure 1.

There are three parameters in this system of equations, namely $Rb = U/(s_0\Omega)$, $Fr = U/(s_0 g)^{1/2}$ and $We = \rho U^2 a/\sigma$, which are the Rossby, Froude and Weber numbers respectively, where in these expressions U is the exit speed of the jet at the orifice, Ω is the rate of rotation of the container, ρ is the liquid's density, σ is the surface tension of the liquid and g is the acceleration due to gravity. Note that Rb^{-1} represents the dimensionless rotation rate, Fr^{-1} represents the dimensionless gravity and We^{-1} represents the dimensionless surface tension, all relative to the speed of the flow in the jet.

The steady equations were found by Decent *et al.* (2002) to be

$$\begin{aligned}
u_0^2 &= 1 - 2YFr^{-2} + Rb^{-2}\left(X^2 + 2X + Z^2\right) + 2We^{-1}\left(1 - R_0{}^{-1}\right), \\
R_0^2 u_0 &= 1, \\
-\left(Z'X'' - X'Z''\right)Fr^{-2} + 2Y'' u_0 Rb^{-1} &= (X+1)\left(Y''Z' - Z''Y'\right)Rb^{-2} + Z\left(Y'X'' - Y''X'\right)Rb^{-2}, \\
\left(u_0^2 - We^{-1}R_0^{-1}\right)\left(X''^2 + Y''^2 + Z''^2\right) &= 2u_0 Rb^{-1}\left(X'Z'' - Z'X''\right) + Rb^{-2}\left((X+1)X'' + ZZ''\right) - Y''Fr^{-2}, \\
X'^2 + Y'^2 + Z'^2 &= 1
\end{aligned} \tag{1.1}$$

where the dashes denote differentiation with respect to s. The initial conditions of these equations are $X' = R_0 = u_0 = 1$ and $X = Y = Y' = Z = Z' = 0$ at $s = 0$. Wallwork *et al.* (2002) determined these equations in the special case in which $Fr = \infty$ (i.e. neglecting gravity).

The torsion of the centreline of the curved jet is $\kappa_2 = P/Q$ where

$$P = X'\left(-Z''Y''' + Y''Z'''\right) + Z'\left(-Y''X''' + X''Y'''\right) + Y'\left(-X''Z''' + Z''X'''\right), \tag{1.2}$$

$$Q = \left(-Z'Y'' + Y'Z''\right)^2 + \left(Y'X'' - X'Y''\right)^2 + \left(-X'Z'' + Z'X''\right)^2. \tag{1.3}$$

(See Decent *et al.* (2018).)

A numerical solution can be found to equations (1.1) to (1.3) for $O(1)$ values of the parameters. Equations (1.1) can be written as a set of ODEs involving the jet location X, Y and Z. These equations are then solved numerically using a Runge-Kutta scheme with the initial conditions at the nozzle. We utilized the numerical solver ode45 in MATLAB which implements a Runge-Kutta method with a variable integration step. Figure 2 shows the trajectory of a typical curved jet for parameter values $Fr = 1$, $Rb = 1$ and $We = 10$ (such numerical solutions are explored in more detail by Decent *et al.* 2002), and Figure 3 shows the torsion κ_2 plotted against the arclength s for the same parameter values. This curve for the torsion is found to be typical, with an initially negative value for the torsion at the orifice and with the torsion tending slowly towards zero for large s. It can be seen that the torsion κ_2 is not asymptotically large for these parameter values for any value of s.

Wallwork *et al.* (2002) and Decent *et al.* (2002) showed that such jets break-up into droplets for an $O(1)$ value of the arclength s, caused by growing unstable travelling waves that propagate along the jet, and confirmed by comparison with experiments such as by Wong *et al.* (2004), Partridge *et al.* (2005) and Hawkins *et al.* (2010). However observations also indicate that a jet does not form and droplets are produced directly from the orifice for small values of the Weber number We.

This paper examines situations where the torsion may become large, in order to determine if the method developed by Wallwork *et al.* (2002) and Decent *et al.* (2002) remains valid for a slender jet. Decent *et al.* (2018) showed that the torsion may become large at the orifice when $Rb \ll 1$ and so this situation is examined in this paper in detail using an asymptotic method. This paper will show that

even when the torsion is asymptotically large at the orifice, it is only large in a narrow inner region asymptotically close to the orifice and in which the jet is not slender. Outside of this narrow inner region, this paper will show that the jet is described by an outer region in which the jet is slender and in which the torsion is never asymptotically large. Hence the method developed by Wallwork *et al.* (2002) and Decent *et al.* (2002) can always be used even when the torsion becomes asymptotically large at the orifice. This is important because the method developed by Wallwork *et al.* (2002) and Decent *et al.* (2002) has been shown to be straight forward to implement in complex scenarios, while in contrast the rigorous mathematical method of Shikhmurzaev & Sisoev (2017) produces lengthy equations and appear to be more difficult to use even in simple situations.

Equations (1.1) to (1.3) were solved close to the orifice for $s \to 0$ by Decent *et al.* (2018) (valid for all values of the non-dimensional paramaters Rb, Fr and We), giving that

$$\begin{aligned}
X &= s - \frac{We^2\left(Rb^2+4Fr^4\right)}{6Fr^4Rb^2\left(1-We\right)^2}s^3 + O\left(s^4\right),\\
Y &= \frac{We}{2Fr^2\left(1-We\right)}s^2 + \frac{We^3}{Rb^2Fr^2\left(1-We\right)^2\left(2We+1\right)}s^3 + O\left(s^4\right),\\
Z &= \frac{We}{Rb\left(We-1\right)}s^2 - \frac{2We^2}{3Rb^3\left(1-We\right)^2}s^3 + O\left(s^4\right),\\
R_0 &= 1 - \frac{We}{Rb^2\left(2We+1\right)}s + O\left(s^2\right),\\
u_0 &= 1 + \frac{2We}{Rb^2\left(2We+1\right)}s + O\left(s^2\right)
\end{aligned} \tag{1.4}$$

and

$$\kappa_2 = -\frac{4WeFr^2}{Rb\left(2We+1\right)\left(Rb^2+4Fr^4\right)} + \frac{2WeJ}{Rb^3Fr^2\left(4Fr^4+Rb^2\right)^2\left(2We+1\right)^3\left(We-1\right)^2}s + O\left(s^2\right), \tag{1.5}$$

where

$$\begin{aligned}
J = {} & 64Fr^8Rb^2We^4 + 208Fr^8Rb^2We^3 + 144Fr^8Rb^2We^2 + 64Fr^8We^4 + 16Fr^4Rb^4We^4\\
& + 20Fr^8Rb^2We - 168We^3Fr^8 + 100Fr^4Rb^4We^3 - 4Fr^8Rb^2 + 72Fr^8We^2\\
& + 84Fr^4Rb^4We^2 + 32Fr^8We + 17Fr^4Rb^4We - 18Rb^2We^3Fr^4 + 12Rb^6We^3\\
& - Fr^4Rb^4 + 18Fr^4Rb^2We^2 + 12Rb^6We^2 + 3Rb^6We.
\end{aligned} \tag{1.6}$$

The singularity in the above expansions at $We = 1$ is well known e.g. Keller & Geer (1973). Note that Decent *et al.* (2018) only calculated the first term in the above expansion for κ_2. In order to determine the second term shown here it was necessary to determine terms up to and including $O\left(s^4\right)$ in the other expansions, though these terms are not shown here for the purposes of brevity.)

Decent *et al.* (2018) also showed that $\kappa_2 = O\left(s^{-1/2}\right)$ as $s \to \infty$, far from the orifice, so that $\kappa_2 \to 0$ as $s \to \infty$. (This result is valid for all values of the non-dimensional paramaters Rb, Fr and We.) This slow decay of κ_2 towards zero associated with $s^{-1/2}$ can be seen in Figure 3. When κ_2 is examined computationally for much larger values of s (e.g. $s = 1000$) for the parameters shown in Figure 3, then this decay proportional to $s^{-1/2}$ can be confirmed computationally.

When the parameters Rb, Fr and We are $O(1)$, the torsion κ_2 is always found to be $O(1)$ or small, and so the asymptotic method developed by Wallwork *et al.* (2002) and Decent *et al.* (2002) is always accurate (because of Decent *et al.* 2018). As pointed out by Decent *et al.* (2018) and as can be seen from equation (1.5), the torsion κ_2 is asymptotically large close to the orifice when $Rb \ll 1$. In such situations there are steep gradients in the solutions close to $s = 0$ (as can be seen in (1.4)) and a numerical solution is not the most appropriate method to fully understand the behaviour of (1.1) for $Rb \ll 1$. This paper therefore examines asymptotic solutions to equations (1.1) using the limit $Rb \to 0$ and examines three different scenarios: (i) $Fr = O(1)$; (ii) $Fr = O\left(\sqrt{Rb}\right)$; and (iii) $Fr = O(Rb)$. These three scenarios are motivated by different asymptotic balances inherent in (1.5) and are considered in the following three sections of this paper. When $Rb \ll 1$ and $Fr = O(1)$ then $\kappa_2 = O\left(Rb^{-1}\right)$ from (1.5). When $Rb \ll 1$ and $Fr = O\left(\sqrt{Rb}\right)$ then $\kappa_2 = O\left(Rb^{-2}\right)$ from (1.5), and the term $Rb^2 + 4Fr^4$ in (1.5) is asymptotically balanced. When $Rb \ll 1$ and $Fr = O(Rb)$ then $\kappa_2 = O\left(Rb^{-1}\right)$ from (1.5), and there is an asymptotic balance between the term $Rb^2 + 4Fr^4$ and the term Fr^2 in (1.5). In each case, an inner region close to the orifice at $s = 0$ is identified, as well as an outer region for $s = O(1)$. [illegible]periments show that travelling waves propagate along the jet when $s = O(1)$ and cause the jet to r[illegible]e, and hence this is a feature associated primarily with the outer region.)

The limit of $Rb \ll 1$ takes the model into an extreme scenario at especially high rotation rate. For example, in the experiments by Wallwork *et al.* (2002), the rotation rate was around 100 revolutions per minute (r.p.m.), while it would have needed to be about 10,000 r.p.m. for $Rb \ll 1$, as discussed by Decent *et al.* (2018). By examining the model in such extremes, this paper demonstrates that the method developed by Wallwork *et al.* (2002) and Decent *et al.* (2002) is valid in an outer region for $s = O(1)$ in each case, however large the torsion is at the orifice, since the torsion will be found here to be $O(1)$ or smaller in the outer regions. This observation is important since the method developed by Wallwork *et al.* (2002) and Decent *et al.* (2002) has been shown to be straight forward to implement in various complex scenarios (e.g. examining non-Newtonian liquids, compound jets with multiple liquids, liquids with surfactants), and this paper shows that it can be used in an outer region where the jet is slender and where the jet usually becomes unstable and ruptures, even when $Rb \ll 1$. This paper will also show that the jet is not slender in the inner region where the torsion can become asymptotically large.

2. Asymptotic scenario 1: $Rb \ll 1$ and $Fr = O(1)$

This section considers $Rb \ll 1$ and $Fr = O(1)$, and examines an inner region close to the orifice and matches to an outer region where $s = O(1)$.

2.1 *Inner region*

Examining equations (1.1) for $Rb \to 0$ and $Fr = O(1)$, it can be seen from (1.4) that there are steep gradients in the variables as s increases from zero when $Rb \to 0$. The equations are rescaled in an inner region close to $s = 0$ using $X = \hat{X}Rb^m$, $Y = \hat{Y}Rb^p$, $Z = \hat{Z}Rb^q$ and $s = \bar{s}Rb^n$ where m, n, p and q are positive constants to be determined. (In this subsection, which describes this inner region, dashes now denote differentiation with respect to $\bar{s}$, and also subsequently when inner regions are discussed throughout this paper.)

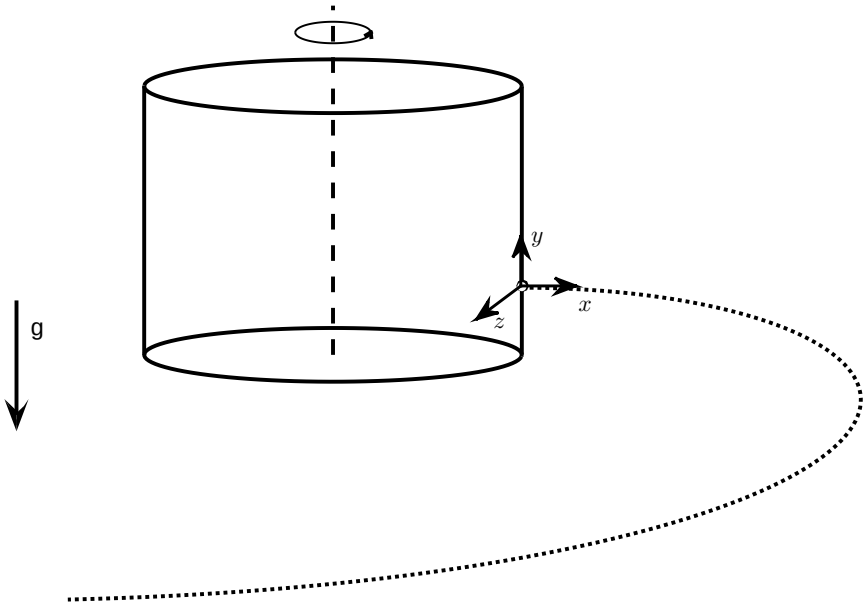

FIG. 1. Sketch of the flow and coordinate system showing the rotating cylinder, which rotates anti-clockwise about its central axis. The centreline of the liquid jet is shown by the dashed line. The x, y, z coordinate system is shown, and the coordinate system rotates with the cylinder. The centreline of the jet is given by the curve $x = X(s)$, $y = Y(s)$ and $z = Z(s)$. The direction of gravity is also shown.

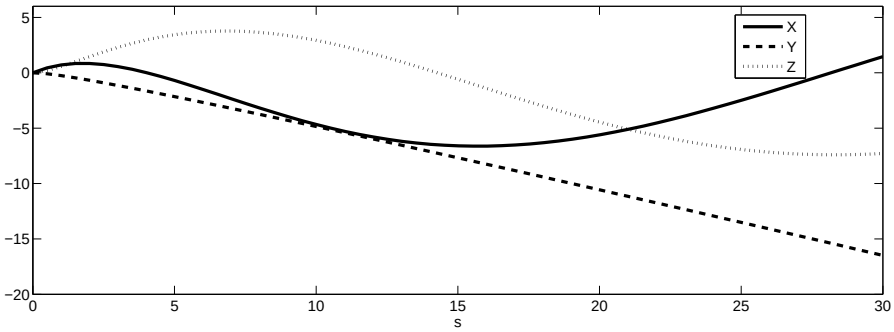

FIG. 2. The trajectory of a rotating liquid jet for $Fr = 1$, $Rb = 1$ and $We = 10$. The graph shows X (solid line), Y (dashed line) and Z (dotted line) plotted against arclength s. The jet's centreline will be at $x = X(s)$, $y = Y(s)$ and $z = Z(s)$. The jet's centreline is rotating around the container and hence X and Z can be seen to be both positive and negative as the jet spirals away from the container. The jet does not intersect again with the container, after it leaves the orifice at $s = 0$, as it spirals away. The vertical coordinate Y can be seen to be approximately linear as the jet falls under gravity.

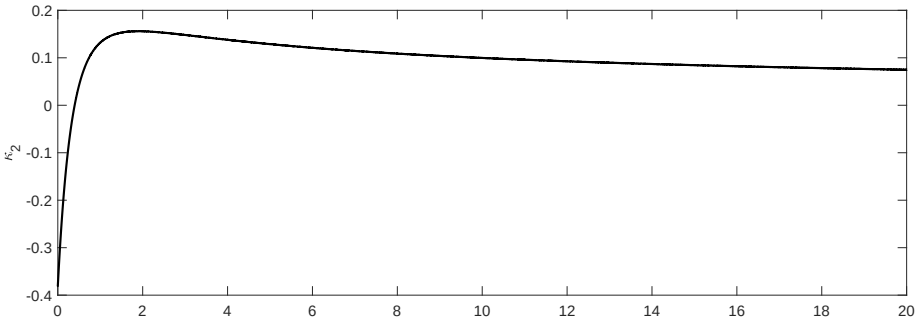

FIG. 3. The torsion κ_2 plotted against the arclength s for $Fr = 1$, $Rb = 1$ and $We = 10$.

From the equation for u_0 in (1.1), $m = 2$ so that u_0 varies with $\bar{s}$ at leading order and also so that $u_0 = O(1)$ in this inner region which is required since $u_0 = 1$ at $s = 0$. Since $X' = 1$ at $s = 0$ then $X' = O(1)$ in this inner region, and also examining the last of the five equations in (1.1) it can thus be seen that $n = 2$. Then the leading-order terms from the small s asymptotic expansions for Y and Z in (1.4) show that $p = 4$ and $q = 3$.

We pose asymptotic series using $u_0 = U_0(\bar{s}) + U_2(\bar{s})\,Rb^2 + O\left(Rb^4\right)$, $R_0 = r_0(\bar{s}) + r_2(\bar{s})\,Rb^2 + O\left(Rb^4\right)$, $\hat{X} = X_0(\bar{s}) + X_2(\bar{s})\,Rb^2 + O\left(Rb^4\right)$, $\hat{Y} = Y_0(\bar{s}) + Y_2(\bar{s})\,Rb^2 + O\left(Rb^4\right)$ and $\hat{Z} = Z_0(\bar{s}) + Z_2(\bar{s})\,Rb^2 + O\left(Rb^4\right)$. Then $(X_0')^2 = 1$ from the final equation in (1.1). Since $X_0' = 1$ and $X_0 = 0$ at $\bar{s} = 0$ then $X_0 = \bar{s}$. Therefore, (1.1) gives that

$$\begin{aligned} U_0^2 &= 1 + 2\bar{s} + 2We^{-1}\left(1 - {r_0}^{-1}\right), \\ r_0^2 U_0 &= 1, \\ 2X_2' + Z_0'^2 &= 0, \\ \left(U_0^2 - We^{-1} r_0^{-1}\right) Z_0'' &= 2U_0 - Z_0', \\ Fr^{-2} + \left(U_0^2 - We^{-1} r_0^{-1}\right) Y_0'' + Y_0' &= 0. \end{aligned} \tag{2.1}$$

These inner region equations (2.1) need to be solved subject to $X_2 = X_2' = Y_0 = Y_0' = Z_0 = Z_0' = 0$ at $\bar{s} = 0$.

Note that from (1.2) and (1.3), $P = O\left(Rb^{-3}\right)$ and $Q = O\left(Rb^{-2}\right)$ in the inner region. Hence the torsion $\kappa_2 = O\left(Rb^{-1}\right)$ in the inner region.

Equations (2.1) can be solved for $\bar{s} \to 0$. This gives $U_0 = 1 + 2We(2We+1)^{-1}\bar{s} + O\left(\bar{s}^2\right)$, $r_0 = 1 - We(2We+1)^{-1}\bar{s} + O\left(\bar{s}^2\right)$, $X_2 = -2We^2(We-1)^{-2}\bar{s}^3/3 + O\left(\bar{s}^4\right)$, $Y_0 = -WeFr^{-2}(We-1)^{-1}\bar{s}^2/2 + We^3 Fr^{-2}(2We+1)^{-1}(We-1)^{-2}\bar{s}^3 + O\left(\bar{s}^4\right)$ and $Z_0 = We(We-1)^{-1}\bar{s}^2 - 2We^2(We-1)^{-2}\bar{s}^3/3 + O\left(\bar{s}^4\right)$. These agree with (1.4) for $Rb \to 0$. Determining the torsion κ_2 in the inner region for $\bar{s} \to 0$ using (1.2), (1.3) and $Rb \to 0$, gives $\kappa_2 = -WeRb^{-1}Fr^{-2}(2We+1)^{-1} + O(\bar{s})$ which agrees with (1.5) for $Rb \to 0$. As expected, the torsion is $O\left(Rb^{-1}\right)$ in the inner region for $\bar{s} \to 0$. Therefore, this asymptotic expansion for small $\bar{s}$ confirms agreement with (1.4) and (1.5), confirms the initial asymptotic size of the torsion at the orifice, and provides results that can be used to confirm the numerical solutions for the inner region in section 2.3.

Equations (2.1) can also be solved for $\bar{s} \to \infty$. By seeking leading-order terms for each of the variables in the form of a constant times by $\bar{s}^{constant}$, and seeking the largest terms as $\bar{s} \to \infty$, and

then seeking higher-order terms, gives $U_0 = \sqrt{2\bar{s}} - We^{-1}(2\bar{s})^{-1/4} + \sqrt{2}\left(1+2We^{-1}\right)(16\bar{s})^{-1/2} + ...$, $r_0 = (2\bar{s})^{-1/4} + (4We\bar{s})^{-1} + ...$, $X_2 = -\bar{s}^2/2 + ...$, $Y_0 = -Fr^{-2}\bar{s} + \tilde{Y}\bar{s}^{1/2} + ...$ and $Z_0 = 2\sqrt{2}\bar{s}^{3/2}/3 + ...$ In this equation for Y_0, $\tilde{Y}$ is a constant which cannot be determined from the $\bar{s} \to \infty$ asymptotics and must be found from a numerical solution to (2.1) in the inner region, and so $\tilde{Y}$ will depend upon the parameters We and Fr. The torsion can be determined in the inner region for $\bar{s} \to \infty$ using (1.2), (1.3) and $Rb \to 0$ which is found to be $\kappa_2 = -\sqrt{2}\tilde{Y}Rb^{-1}(2\bar{s})^{-2} + ...$ so that $\kappa_2 \to 0$ as $\bar{s} \to \infty$. Note that this expression for the torsion contains Rb, and so $\kappa_2 = O\left(Rb^{-1}\right)$ as it is throughout the inner region, but also note that the torsion tends to zero for large $\bar{s}$. Consequently note that the torsion κ_2 is $O\left(Rb^{-1}\right)$ at $\bar{s} = 0$ at the start of the inner region, but has tended to zero as $\bar{s} \to \infty$ at the other side of the inner region.

Equations (2.1) can be solved exactly at leading order in the limit $We \to \infty$ giving $U_0 = \sqrt{1+2\bar{s}}$, $r_0 = (1+2\bar{s})^{-1/4}$, $X_2 = \bar{s}(1-\bar{s})/2 - \ln(1+2\bar{s})/4$, $Y_0 = Fr^{-2}\left(\sqrt{2\bar{s}+1} - \bar{s} - 1\right)$ and $Z_0 = (2\bar{s}+1)^{3/2}/3 - \sqrt{2\bar{s}+1} + 2/3$. This also shows that $\tilde{Y} = \sqrt{2}Fr^{-2}$ for $We \to \infty$. The torsion κ_2 can now be determined exactly throughout the inner region for $We \to \infty$. Expanding P and Q in terms of Rb using (1.2) and (1.3), the torsion is found to be

$$\kappa_2 = \frac{Y_0''Z_0''' - Y_0'''Z_0''}{Rb\left(Z_0''\right)^2} + ... \tag{2.2}$$

at leading-order in Rb, which is valid for $We = O(1)$ and for $We \to \infty$. Therefore, the torsion in the inner region for $We \to \infty$ is given by $\kappa_2 = -Rb^{-1}Fr^{-2}(1+\bar{s})^{-2}/2 + ...$ for $Rb \to 0$. Therefore, the torsion κ_2 increases from its initial value at $\bar{s} = 0$ and tends to zero as $\bar{s} \to \infty$.

Since (1.4) have a singularity at $We \to 1$, it is interesting to examine the limit $We \to 1$ in this inner region in order to understand what the singularity does to the torsion κ_2. A further asymptotic region can be identified close to $\bar{s} = 0$ in this limit, which is examined using $\bar{s} = \alpha\tilde{s}$ and $We = 1 + \omega\alpha$ where $\alpha \to 0$, $\alpha > 0$ and $\omega = \pm 1$, so that $We > 1$ when $\omega = 1$, and $We < 1$ when $\omega = -1$. Then equations (2.1) give that $U_0 = 1 + 2\tilde{s}\alpha/3 + \tilde{s}\alpha^2(2\omega - \tilde{s})/9 + O\left(\alpha^3\right)$ and $r_0 = 1 - \tilde{s}\alpha/3 + \tilde{s}\alpha^2(2\tilde{s} - \omega)/9 + O\left(\alpha^3\right)$. We expand $Y_0 = \alpha\tilde{Y}_1(\tilde{s}) + \alpha^2\tilde{Y}_2(\tilde{s}) + O\left(\alpha^3\right)$ and $Z_0 = \alpha\tilde{Z}_1(\tilde{s}) + \alpha^2\tilde{Z}_2(\tilde{s}) + O\left(\alpha^3\right)$. Then (2.1) gives that $\tilde{Y}_1 = -Fr^{-2}\tilde{s} + \omega Fr^{-2}\ln|\tilde{s} + \omega|$ and $\tilde{Z}_1 = 2\tilde{s} - 2\omega\ln|\tilde{s} + \omega|$. The torsion can be calculated to be $\kappa_2 = -(1+\omega\tilde{s})Fr^{-2}Rb^{-1}/3 + O(\alpha)$ as $\alpha \to 0$. Note that when $We < 1$ in this region (i.e. for $\omega = -1$) then there are singularities in Y_0 and Z_0 at $\tilde{s} = 1$. Though there are no singularities in the solution for Y_0 and Z_0 (in the physical domain of the jet for $\tilde{s} \geqslant 0$) for $We > 1$ (i.e. for $\omega = 1$). However, κ_2 is not singular in this region for $\omega = 1$ or $\omega = -1$. Also note that $\kappa_2 = 0$ at $\tilde{s} = 1$ when $\omega = -1$. This set of asymptotics for $We \to 1$ could be further examined asymptotically close to $\tilde{s} = 1$, however it has been shown here that the torsion $\kappa_2 \to 0$ (rather than becoming large) as $\tilde{s} \to 1$ for $We < 1$ and hence this is not relevant in the context of this paper where we are concerned with situations when the torsion becomes large. Also experiments show (e.g. Wong *et al.* 2004) that for small We the jets are short and break-up at the orifice.

2.2 *Outer region*

An outer region is now examined where $s = O(1)$. Taking the far-field of the inner region and using $\bar{s} = sRb^{-2}$ gives that $u_0 = \sqrt{2s}/Rb + ...$, $R_0 = \sqrt{Rb}(2s)^{-1/4} + ...$, $X = s + ...$, $Y = -Rb^2Fr^{-2}s + ...$ and $Z = 2\sqrt{2}s^{3/2}/3 + ...$ in the far-field of the inner region. These expressions are then the small s asymptotics for the outer region, and these equations can be used to determine the expansions in the outer region. That is, the first terms in expansions in Rb in the outer region are given by $u_0 = Rb^{-1}U + ...$, $R_0 = \sqrt{Rb}R + ...$ and $Y = Rb^2\bar{Y} + ...$ as $Rb \to 0$, while X and Z are $O(1)$ at leading-order in Rb in the

outer region. Substituting these into equations (1.1) and taking $Rb \to 0$ gives the leading-order equations in the outer region as

$$\begin{aligned} U &= \sqrt{X^2+2X+Z^2}, \\ R &= \left(X^2+2X+Z^2\right)^{-1/4}, \\ \left(Z'X''-X'Z''\right)Fr^{-2} &= 2\bar{Y}''U-(X+1)\left(\bar{Y}''Z'-Z''\bar{Y}'\right)-Z\left(\bar{Y}'X''-\bar{Y}''X'\right), \\ U^2\left(X''^2+Z''^2\right) &= 2U\left(X'Z''-Z'X''\right)+(X+1)X''+ZZ'', \\ X'^2+Z'^2 &= 1. \end{aligned} \tag{2.3}$$

The initial conditions for these outer region equations are obtained from the small s asymptotics in the outer region. Note that the Weber number We does not appear in these leading-order outer region equations (2.3).

The above outer region equations (2.3) for X, Z, U and R are the two-dimensional steady jet trajectory equations from Wallwork et al (2002) for small Rb, which correspond to the problem without gravity (i.e. $Fr=\infty$), together with an additional equation for $\bar{Y}$ that has decoupled from the other equations in the outer region. Thus the outer region has become equivalent to the two-dimensional planar equations for the jet trajectory, with an additional equation which gives the smaller fall caused by gravity described by $\bar{Y}$.

The asymptotic size of the torsion κ_2 in the outer region can be found from (1.2) and (1.3), noting that $Y=O\left(Rb^2\right)$ in the outer region. Equations (1.2) and (1.3) give that $P=O\left(Rb^2\right)$ and $Q=O(1)$ where $Rb\to 0$. Therefore, $\kappa_2=O\left(Rb^2\right)$ in the outer region and thus the torsion is small throughtout the outer region.

Equations (2.3) can be solved for $s\to\infty$ by introducing two new functions $r(s)$ and $\theta(s)$ by writing X and Z using $X=r(s)\cos(\theta(s))-1$ and $Z=r(s)\sin(\theta(s))$. Substituting these into (2.3) and seeking a solution for large s gives that $r=\zeta\sqrt{s}+\ldots$ and $\theta=\gamma\sqrt{s}+\ldots$ as $s\to\infty$, where ζ and γ are $O(1)$ constants and $\zeta\gamma=2$. Thus ζ and γ are related, and they would be determined from solving (2.3) numerically. Solving the equation for $\bar{Y}$ in (2.3) for large s using these solutions for X and Z gives that $\bar{Y}=-\gamma^2Fr^{-2}s/2+\ldots$ as $s\to\infty$. These large s asymptotics can then be used to show that the torsion $\kappa_2=Rb^2\gamma^3Fr^{-2}s^{-1/2}/4+\ldots$ as $s\to\infty$ using (1.2) and (1.3). Therefore, the torsion $\kappa_2\to 0$ as $s\to\infty$.

2.3 *Numerical solutions in the inner and outer regions*

Figures 4, 5 and 6 show the torsion κ_2 plotted against the arclength $\bar{s}$, calculated computationally from the inner region equations (2.1) for the scalings used in this section, shown for various parameter values. (Equation (2.2) is used to determine the torsion κ_2.) Figure 4 shows how κ_2 varies with Fr for $We=10$ and $Rb=0.01$, showing curves for κ_2 for $Fr=0.5,1$ and 3. It can be seen that the torsion κ_2 increases along each curve from an initially negative value and tends to zero in the far-field for large $\bar{s}$.

Figure 5 shows how κ_2 varies with We for $Rb=0.01$ and $Fr=1$, showing curves for κ_2 for $We=2,3$ and 100. Again, κ_2 increases along each curve and tends to zero in the far-field. However, it can be seen in Figure 5 that varying We does not cause significant changes to the torsion in this case.

Figure 6 shows how κ_2 varies with three smaller values of We for $Rb=0.01$ and $Fr=1$, showing curves for κ_2 for $We=0.2,0.5$ and 3. Figure 6 shows that the torsion heads towards $\kappa_2=0$ at a singularity at a finite value of $\bar{s}$ for the two curves on which $We<1$, namely $We=0.2$ and 0.5, in keeping with the behaviour identified for $We\to 1$ for $We<1$ in subsection 2.1. However, for $We=3$, there is no singularity and the solution tends to zero as $\bar{s}$ increases to infinity. Note though that the large

$\bar{s}$ behaviour for κ_2 is similiar for $We = 0.2$ and $We = 3$ until the curve for $We = 0.2$ hits the singularity and the curve halts at $\kappa_2 = 0$. We know from the $We \to 1$ asymptotics in this section for $We < 1$ that the singuarity can be integrated through. Note that Wallwork *et al.* (2002) and Wong *et al.* (2004) showed in laboratory experiments that a coherent jet is usually not formed for $We < 1$ and break-up occurs close to the orifice, and so it is likely that the jet will break-up before the singularity at $\kappa_2 = 0$ is reached.

The behaviour of Y_0 and Z_0 plotted against arclength $\bar{s}$ in the inner region is shown in Figures 7 and 8 respectively, which each show Y_0 and Z_0 for $We = 0.5$ and $We = 2$ for $Fr = 1$. These curves are found by solving (2.1) numerically. For $We < 1$, a singularity is found in the solution for Y_0 and Z_0 at finite $\bar{s}$ and this corresponds to the value of $\bar{s}$ at which $\kappa_2 = 0$ (compare to Figure 6). For $We > 1$, the solution does not have a singularity. Note also that the jet flows upwards initially after leaving the orifice when $We < 1$ (see figure 7), in line with the small s asymptotics in (1.4).

The outer region equations (2.3) can also be solved numerically. This numerical solution is shown in Figure 9 for $Fr = 1$. The solid line shows $r(s)$, the dashed line shows $\theta(s)$ and the dotted line shows $\bar{Y}(s)$, where $X = r(s)\cos(\theta(s)) - 1$ and $Z = r(s)\sin(\theta(s))$. It can be seen that the jet's trajectory falls under gravity (since $\bar{Y}$ is negative and decreasing) and the jet spirals away from the orifice (since r and θ are increasing).

In summary, this section has identified an inner and outer solution, where the torsion is only asymptotically large in the inner region and the torsion decays to become small as it approaches the outer region. Two cases, $We \to \infty$ and $We \to 1$, were also examined. For $We \to \infty$, the inner region equations could be solved analytically without using a numerical solution, confirming the features observed in the numerical solutions. For $We \to 1$, it was shown that there is a singularity in the solution for $We < 1$ at which κ_2 approaches zero, and this feature is also found in the numerical solutions for $We < 1$, and so we note that the torsion κ_2 does not become large at this singularity.

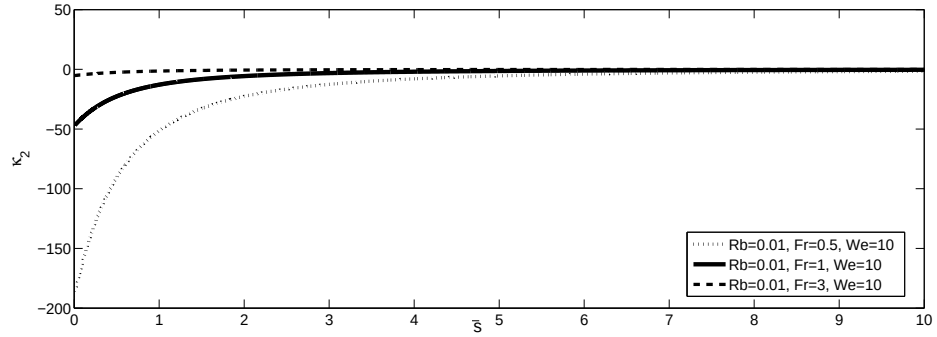

FIG. 4. Torsion κ_2 plotted against $\bar{s}$ for various values of the Froude number ($Fr = 0.5, 1$ and 3) in the inner region for section 2. The other parameters are $Rb = 0.01$ and $We = 10$.

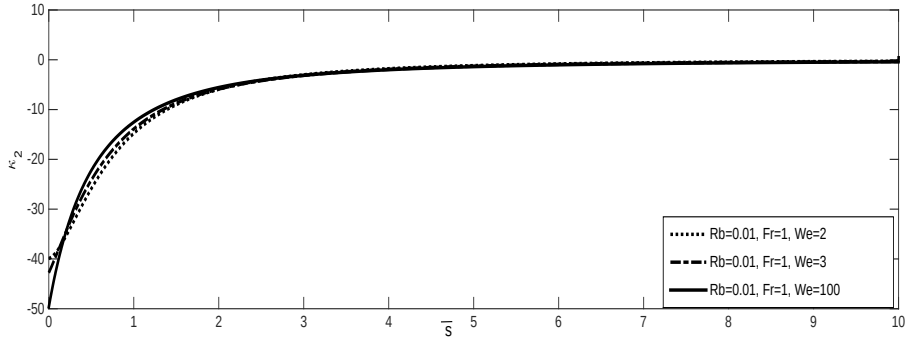

FIG. 5. Torsion κ_2 plotted against $\bar{s}$ for various values of the Weber number ($We = 2, 3$ and 100) in the inner region for section 2. The other parameters are $Rb = 0.01$ and $Fr = 1$.

3. Asymptotic scenario 2: $Rb \ll 1$ and $Fr = O\left(\sqrt{Rb}\right)$

This section examines $Rb \to 0$ and $Fr \to 0$. If $Fr^2 = O(Rb)$ as $Rb \to 0$ then the term $Rb^2 + 4Fr^4$ in equation (1.5) will be asymptotically balanced and so this appears to be an important limit for the consideration of the torsion. Therefore, the equations are rescaled in an inner region close to $s = 0$ using $X = \hat{x}Rb^m$, $Y = \hat{y}Rb^p$, $Z = \hat{z}Rb^q$, $s = \bar{s}Rb^n$ and $Fr^2 = f^2Rb$ where m, n, p and q are positive constants which are taken to be the same as in the previous section so that $m = n = 2$, $p = 4$ and $q = 3$. Also $f = O(1)$ is a parameter. Expanding using $u_0 = \hat{U}_0(\bar{s}) + O(Rb)$, $R_0 = \hat{r}_0(\bar{s}) + O(Rb)$, $\hat{x} = \hat{X}_0(\bar{s}) + \hat{X}_2(\bar{s})Rb^2 + O\left(Rb^3\right)$, $\hat{y} = Rb^{-1}\hat{Y}_0(\bar{s}) + O(1)$ and $\hat{z} = \hat{Z}_0(\bar{s}) + O(Rb)$, then $\left(\hat{X}_0{}'\right)^2 = 1$ from the fifth equation in (1.1). Since $\hat{X}_0{}' = 1$ and $\hat{X}_0 = 0$ at $\bar{s} = 0$ then $\hat{X}_0 = \bar{s}$. Therefore, (1.1) gives that

$$\begin{aligned}
\hat{U_0}^2 &= 1 + 2\bar{s} + 2We^{-1}\left(1 - \hat{r_0}^{-1}\right), \\
\hat{r_0}^2\hat{U_0} &= 1, \\
-\hat{Z_0}''f^{-2} - 2\hat{Y_0}''\hat{U_0} + \hat{Y_0}''\hat{Z_0}' &= \hat{Z_0}''\hat{Y_0}', \\
\left(\hat{U_0}^2 - We^{-1}\hat{r_0}^{-1}\right)\left(\hat{Y_0}''^2 + \hat{Z_0}''^2\right) &= -f^{-2}\hat{Y_0}'' + 2\hat{U_0}\hat{Z_0}'' + \hat{X_2}'', \\
2\hat{X_2}' + \hat{Y_0}'^2 + \hat{Z_0}'^2 &= 0.
\end{aligned} \tag{3.1}$$

These inner region equations need to be solved for $\hat{X}_2$, $\hat{Y}_0$ and $\hat{Z}_0$ subject to $\hat{X}_2 = \hat{X_2}' = \hat{Y}_0 = \hat{Y_0}' = \hat{Z}_0 = \hat{Z_0}' = 0$ at $\bar{s} = 0$.

Examining $\bar{s} \to 0$, $\hat{X}_2 = -We^2\left(1 + 4f^4\right)f^{-4}(1 - We)^{-2}\bar{s}^3/6 + O\left(\bar{s}^4\right)$, $\hat{Y}_0 = Wef^{-2}(1 - We)^{-1}\bar{s}^2/2 + We^3f^{-2}(1 - We)^{-2}(2We + 1)^{-1}\bar{s}^3 + O\left(\bar{s}^4\right)$, $\hat{Z}_0 = We(We - 1)^{-1}\bar{s}^2 - 2We^2(1 - We)^{-2}\bar{s}^3/3 + O\left(\bar{s}^4\right)$, $\hat{r_0} = 1 - We(2We + 1)^{-1}\bar{s} + O\left(\bar{s}^2\right)$, $\hat{U}_0 = 1 + 2We(2We + 1)^{-1}\bar{s} + O\left(\bar{s}^2\right)$ and, using (1.2) and (1.3), $\kappa_2 = -4Wef^2Rb^{-2}(2We + 1)^{-1}\left(1 + 4f^4\right)^{-1} + O(\bar{s})$.

As in the previous section the equations can also be solved for $\bar{s} \to \infty$. This gives $\hat{U}_0 = \sqrt{2\bar{s}} - We^{-1}(2\bar{s})^{-1/4} + \sqrt{2}(1 + 2/We)(16\bar{s})^{-1/2} + ...$, $\hat{r_0} = (2\bar{s})^{-1/4} + (4We\bar{s})^{-1} + ...$, $\hat{X}_2 = -\bar{s}^2/2 + ...$, $\hat{Y}_0 = -f^{-2}\bar{s} + \tilde{y}\bar{s}^{1/2} + ...$ and $\hat{Z}_0 = 2\sqrt{2}\bar{s}^{3/2}/3 + ...$ Here $\tilde{y}$ is a constant which cannot be found from the far-field asymptotics but would be found from a numerical solution of the inner region equations, and

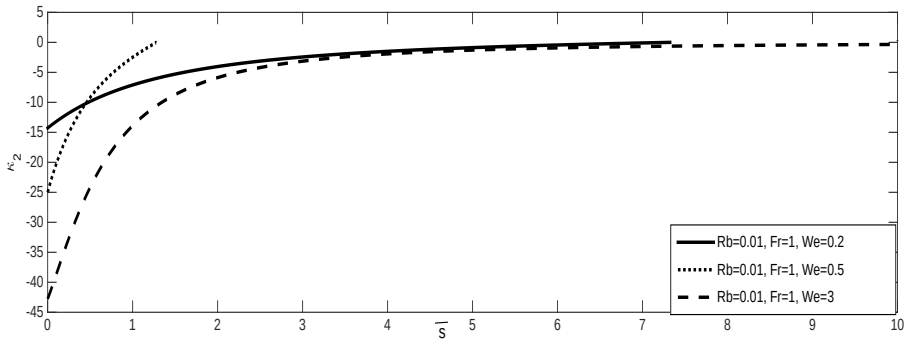

FIG. 6. Torsion κ_2 plotted against $\bar{s}$ for various values of the Weber number ($We = 0.2, 0.5$ and 3) in the inner region for section 2. The other parameters are $Rb = 0.01$ and $Fr = 1$.

so that $\tilde{y}$ will depend upon We and f. The torsion can be determined in the inner region for $\bar{s} \to \infty$ using (1.2), (1.3) and $Rb \to 0$, and is found to be $\kappa_2 = -\sqrt{2}\tilde{y}Rb^{-2}(2\bar{s})^{-2} + ...$ so that $\kappa_2 \to 0$ as $\bar{s} \to \infty$. The torsion κ_2 is $O\left(Rb^{-2}\right)$ at $\bar{s} = 0$ at the start of the inner region, but has tended to zero as $\bar{s} \to \infty$ at the far-field of the inner region.

To determine the equations in the outer region in this section, we again consider the far-field asymptotics of the inner region written in terms of s. This gives $u_0 = \sqrt{2s}Rb^{-1} + ...$, $R_0 = \sqrt{Rb}(2s)^{-1/4} + ...$, $X = s + ...$, $Y = -Rbf^{-2}s + ...$ and $Z = 2\sqrt{2}s^{3/2}/3 + ...$ for the far-field of the inner region, which are then the small s asymptotics for the outer region. Therefore, in the outer region it is necessary to use the leading-order expansions in Rb as $u_0 = Rb^{-1}\bar{V} + ...$, $R_0 = \sqrt{Rb}\bar{S} + ...$ and $Y = Rb\bar{y} + ...$ as $Rb \to 0$, while X and Z are $O(1)$ at leading-order in Rb. Substituting these into equations (1.1), together with $Fr^2 = f^2Rb$, and taking $Rb \to 0$, gives the leading-order equations in the outer region as

$$\begin{aligned}
\bar{V} &= \sqrt{X^2 + 2X + Z^2}, \\
\bar{S} &= \left(X^2 + 2X + Z^2\right)^{-1/4}, \\
\left(Z'X'' - X'Z''\right)f^{-2} &= 2\bar{y}''\bar{V} - (X+1)\left(\bar{y}''Z' - Z''\bar{y}'\right) - Z\left(\bar{y}'X'' - \bar{y}''X'\right), \\
\bar{V}^2\left(X'^2 + Z'^2\right) &= 2\bar{V}\left(X'Z'' - Z'X''\right) + (X+1)X'' + ZZ'', \\
X'^2 + Z'^2 &= 1.
\end{aligned} \tag{3.2}$$

Note these are similar to the outer region equations in the previous section (in which $Fr = O(1)$), but Y is scaled differently in this region. (Compare (3.2) with (2.3).) The initial conditions for these outer region equations are obtained from the above small s asymptotics for the outer region.

Here $P = O(Rb)$ and $Q = O(1)$ in the outer region, so that the torsion $\kappa_2 = O(Rb)$ in the outer region in this section. We can determine the torsion in the far-field of the outer region using the same method as in section 2, which gives in this region $\kappa_2 = Rb\gamma^3 f^{-2}s^{-1/2}/4 + ...$ as $s \to \infty$, where γ is an $O(1)$ constant. Therefore, the torsion $\kappa_2 \to 0$ as $s \to \infty$.

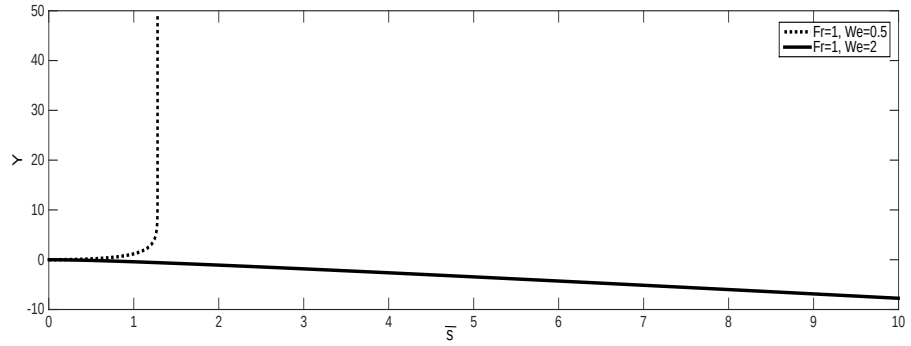

FIG. 7. Y_0 plotted against $\bar{s}$ for $We = 0.5$ and 2 at $Fr = 1$. These curves are solutions to (2.1).

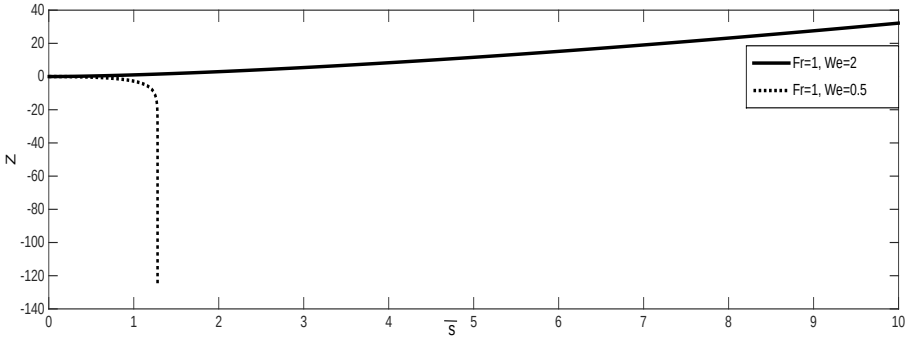

FIG. 8. Z_0 plotted against $\bar{s}$ for $We = 0.5$ and 2. These curves are solutions to (2.1).

Finally note that the equations in the inner region in this section (3.1) can be solved exactly in the combined limit $We \to \infty$ and $f \to \infty$. This gives at leading-order in f and We the solutions $\hat{U}_0 = \sqrt{1+2\bar{s}}$, $\hat{X}_2 = \bar{s}/2 - \bar{s}^2/2 - \ln(1+2\bar{s})/4$, $\hat{Y}_0 = f^{-2}\left(-\bar{s} + \sqrt{1+2\bar{s}} - 1\right)$ and $\hat{Z}_0 = 2\bar{s}\sqrt{1+2\bar{s}} - 2(1+2\bar{s})^{3/2}/3 + 2/3$. This gives $\kappa_2 = -Rb^{-2} f^{-2} (1+\bar{s})^{-2}/2$ in the inner region in this combined limit $We \to \infty$ and $f \to \infty$.

In summary, this section has again identified inner and outer regions, where the torsion is only asymptotically large in the inner region. The torsion is small in the outer region, despite the fact that the torsion $\kappa_2 = O\left(Rb^{-2}\right)$ at the orifice and thus asymptotically larger at the orifice than in section 2. The outer region equations were found to be similar to those found in section 2. The inner region equations were also solved exactly in the limit $We \to \infty$ and $f \to \infty$, and the results confirmed the observations in this section.

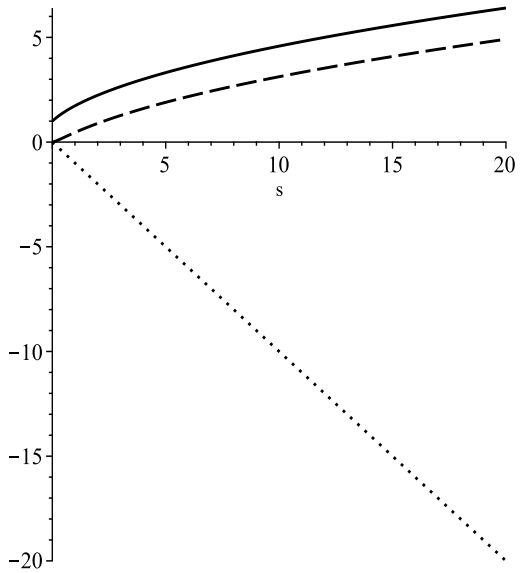

FIG. 9. Numerical solution to outer region equations (2.3) for $Fr = 1$. The solid line shows $r(s)$, the dashed line shows $\theta(s)$ and the dotted line shows $\bar{Y}(s)$, where $X = r(s)\cos(\theta(s)) - 1$ and $Z = r(s)\sin(\theta(s))$.

4. Asymptotic scenario 3: $Rb \ll 1$ and $Fr = O(Rb)$

This section again examines $Rb \to 0$ and $Fr \to 0$. If $Fr = O(Rb)$ as $Rb \to 0$ then there will be an asymptotic balance in the first term in equation (1.5) between terms in the denominator (i.e. $Rb^2 + 4Fr^4$) and numerator (i.e. Fr^2), and so this appears to be an important limit for the consideration of the torsion. Therefore, the equations are rescaled in an inner region close to $s = 0$ using $X = \tilde{x}Rb^m$, $Y = \tilde{y}Rb^p$, $Z = \tilde{z}Rb^q$, $s = \bar{s}Rb^n$ and $Fr = \hat{f}Rb$ where m, n, p and q are positive constants which are taken to be the same as in section 2 so that $m = n = 2$, $p = 4$ and $q = 3$. Also $\hat{f} = O(1)$ is a parameter. Expanding using $u_0 = \tilde{U}_0(\bar{s}) + O\left(Rb^2\right)$, $R_0 = \tilde{r_0}(\bar{s}) + O\left(Rb^2\right)$, $\tilde{x} = x_0(\bar{s}) + O\left(Rb^2\right)$, $\tilde{y} = Rb^{-2}y_0(\bar{s}) + O(1)$ and $\tilde{z} = z_0(\bar{s}) + O\left(Rb^2\right)$ gives

$$\begin{aligned}
{\tilde{U_0}'}^2 &= 1 - 2y_0\hat{f}^{-2} + 2x_0 + 2We^{-1}\left(1 - {\tilde{r_0}}^{-1}\right), \\
{\tilde{r_0}}^2\tilde{U_0} &= 1, \\
\left(z_0'x_0'' - x_0'z_0''\right)\hat{f}^{-2} &= 2y_0''\tilde{U_0} - y_0''z_0' + z_0''y_0', \\
\left({\tilde{U_0}}^2 - We^{-1}{\tilde{r_0}}^{-1}\right)\left(x_0''^2 + y_0''^2\right) &= -\hat{f}^{-2}y_0'' + x_0'', \\
x_0'^2 + y_0'^2 &= 1.
\end{aligned} \tag{4.1}$$

These inner region equations need to be solved for x_0, y_0 and z_0 subject to $x_0' = 1$ and $x_0 = y_0 = y_0' = z_0 = z_0' = 0$ at $\bar{s} = 0$.

Examining $\bar{s} \to 0$ gives $x_0 = \bar{s} - We^2 \hat{f}^{-4}(1-We)^{-2}\bar{s}^3/6 + O(\bar{s}^4)$, $y_0 = We\hat{f}^{-2}(1-We)^{-1}\bar{s}^2/2 + We^3\hat{f}^{-2}(1-We)^{-2}(2We+1)^{-1}\bar{s}^3 + O(\bar{s}^4)$, $z_0 = We(We-1)^{-1}\bar{s}^2 - 2We^2(1-We)^{-2}\bar{s}^3/3 + O(\bar{s}^4)$, $\tilde{r_0} = 1 - We(2We+1)^{-1}\bar{s} + O(\bar{s}^2)$, $\tilde{U_0} = 1 + 2We(2We+1)^{-1}\bar{s} + O(\bar{s}^2)$ and, using (1.2) and (1.3), $\kappa_2 = -4We\hat{f}^2 Rb^{-1}(2We+1)^{-1} + O(\bar{s})$.

The equations can also be solved for $\bar{s} \to \infty$. This gives $\tilde{U_0} = \sqrt{2}\left(1+\hat{f}^4\right)^{1/4}\hat{f}^{-1}\sqrt{\bar{s}} + ...$, $\tilde{r_0} = \sqrt{\hat{f}}\left(1+\hat{f}^4\right)^{-1/8}(2\bar{s})^{-1/4} + ...$, $x_0 = \hat{f}^2\bar{s}/\sqrt{1+\hat{f}^4} + \beta\hat{f}^{-2}\bar{s}^{1/2} + ...$, $y_0 = -\bar{s}/\sqrt{1+\hat{f}^4} + \beta\bar{s}^{1/2} + ...$ and $z_0 = 2\sqrt{2}\hat{f}^3\left(1+\hat{f}^4\right)^{-3/4}\bar{s}^{3/2}/3 + ...$ In these equations β is an $O(1)$ constant which cannot be found from the far-field asymptotics but would be found from a numerical solution in the inner region and so will depend upon We and $\hat{f}$. The torsion can be determined in the inner region for $\bar{s} \to \infty$ using (1.2), (1.3) and $Rb \to 0$. From (1.2), $P = -\sqrt{2}\hat{f}\left(1+\hat{f}^4\right)^{-1/4}\beta(2\bar{s})^{-3}Rb^{-5} + ...$, and from (1.3), $Q = \beta^2\left(1+\hat{f}^4\right)Rb^{-4}(2\bar{s})^{-3}\hat{f}^{-4}/2 + \hat{f}^6\left(1+\hat{f}^4\right)^{-3/2}Rb^{-2}(2\bar{s})^{-1} + ...$ where the first two terms of Q have been shown. This is because the first term in Q shown here dominates for large $\bar{s}$ for $1 \ll \bar{s} \ll Rb^{-1}$, but for $\bar{s} \gg Rb^{-1}$ then the second term instead becomes dominant. Therefore, for $1 \ll \bar{s} \ll Rb^{-1}$ then $\kappa_2 = -2\sqrt{2}\hat{f}^5 Rb^{-1}\beta^{-1}\left(1+\hat{f}^4\right)^{-5/4} + ...$, and for $\bar{s} \gg Rb^{-1}$ then $\kappa_2 = -\sqrt{2}\beta\left(1+\hat{f}^4\right)^{5/4}Rb^{-3}(2\bar{s})^{-2}\hat{f}^{-5} + ...$, so that $\kappa_2 \to 0$ as $\bar{s} \to \infty$.

An outer region is now examined where $s = O(1)$. Taking the far-field of the inner region and using $\bar{s} = sRb^{-2}$ gives that $u_0 = \sqrt{2}\left(1+\hat{f}^4\right)^{1/4}Rb^{-1}\hat{f}^{-1}\sqrt{s} + ...$, $R_0 = 2^{-1/4}\sqrt{Rb}\sqrt{\hat{f}}\left(1+\hat{f}^4\right)^{-1/8}s^{-1/4} + ...$, $X = \hat{f}^2 s/\sqrt{1+\hat{f}^4} + ...$, $Y = -s/\sqrt{1+\hat{f}^4} + ...$ and $Z = 2\sqrt{2}\hat{f}^3\left(1+\hat{f}^4\right)^{-3/4}s^{3/2}/3 + ...$ for the far-field of the inner region, which are then the small s asymptotics in the outer region. Therefore, $X = O(1)$, $Y = O(1)$, $Z = O(1)$, $u_0 = O\left(Rb^{-1}\right)$ and $R_0 = O\left(\sqrt{Rb}\right)$ in the outer region for $Fr = O(Rb)$ as $Rb \to 0$. Writing $u_0 = Rb^{-1}V + ...$ and $R_0 = \sqrt{Rb}S + ...$ in the outer region for $Fr = O(Rb)$ as $Rb \to 0$, and substituting these into (1.1), together with $Fr = \hat{f}Rb$ for $Rb \to 0$, gives the leading-order outer region equations

$$\begin{aligned}
V^2 &= -2Y\hat{f}^{-2} + X^2 + 2X + Z^2, \\
S^2V &= 1, \\
\left(Z'X'' - X'Z''\right)\hat{f}^{-2} &= 2Y''V - (X+1)\left(Y''Z' - Z''Y'\right) - Z\left(Y'X'' - Y''X'\right), \\
V^2\left(X''^2 + Y''^2 + Z''^2\right) &= -Y''\hat{f}^{-2} + 2V\left(X'Z'' - Z'X''\right) + (X+1)X'' + ZZ'', \\
X'^2 + Y'^2 + Z'^2 &= 1,
\end{aligned} \tag{4.2}$$

where $\hat{f} = O(1)$. The initial conditions for these outer region equations are obtained from the small s asymptotics in the outer region described above.

Note that in this outer region, $P = O(1)$, $Q = O(1)$ and the torsion $\kappa_2 = O(1)$. The far-field behaviour of these equations can be determined as in the previous two sections to be $\kappa_2 = \gamma^3/\left(4\hat{f}^2\sqrt{s}\right) = O\left(s^{-1/2}\right)$ as $s \to \infty$ in this outer region. Therefore, $\kappa_2 \to 0$ as $s \to \infty$ in the outer region.

The outer region equations (4.2) can be solved numerically. This is shown in Figure 10 for $\hat{f} = 1$. Using $X = r(s)\cos(\theta(s)) - 1$ and $Z = r(s)\sin(\theta(s))$, the solid line shows $r(s)$, the dashed line shows $\theta(s)$ and the dotted line shows $Y(s)$. The trajectory in the outer region spirals away from the rotating container and falls under gravity.

Finally, equations (4.1) in the inner region in this section can be solved exactly in the combined limit $We \to \infty$ and $\hat{f} \to \infty$. This gives at leading-order in $\hat{f}$ and We the solutions $\tilde{U_0} = \sqrt{1+2\bar{s}} + ...$,

$x_0 = \bar{s} + \hat{f}^{-4}\left(-\bar{s}/2 + \sqrt{1+2\bar{s}} - \ln(1+2\bar{s})/4 - 1\right) + ...$, $y_0 = \hat{f}^{-2}\left(-\bar{s} + \sqrt{1+2\bar{s}} - 1\right) + ...$ and $z_0 = 2\bar{s}\sqrt{1+2\bar{s}} - 2(1+2\bar{s})^{3/2}/3 + 2/3 + ...$, where the first two terms of the expansion for x_0 with respect to $\hat{f}$ have been determined. Then $P = -2(1+2\bar{s})^{-3} Rb^{-5}\hat{f}^{-2} + ...$ and $Q = (1+2\bar{s})^{-3} Rb^{-4}\hat{f}^{-4} + 4(\bar{s}+1)^2 Rb^{-2}(1+2\bar{s})^{-3} + ...$, so that $\kappa_2 = -2\hat{f}^2 Rb^{-1} + ...$ at leading-order for $0 \leqslant \bar{s} \ll Rb^{-1}$. Again, because of the ordering of Q, there is a different expression for the torsion for $\bar{s} \gg Rb^{-1}$, which in this case is $\kappa_2 = -\left(2Rb^3\hat{f}^2\bar{s}^2\right)^{-1} + ...$ in the combined limit $We \to \infty$ and $\hat{f} \to \infty$.

In summary, this section has again found inner and outer regions, where the torsion is asymptotically large at the start of the inner region, but the torsion decays to be $O(1)$ in the outer region. The outer region equations were solved numerically, showing the jet spiralling away from the container. The inner region equations were also solved exactly in the limit $We \to \infty$ and $\hat{f} \to \infty$, confirming the observations found elsewhere in this section.

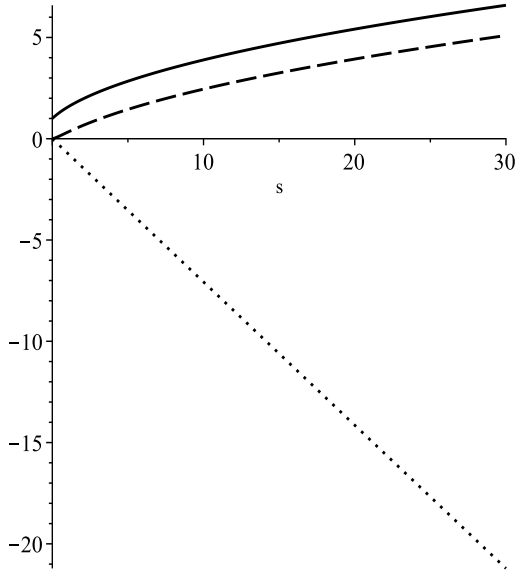

FIG. 10. Numerical solution to outer region equations (4.2) for $\hat{f} = 1$. Using $X = r(s)\cos(\theta(s)) - 1$ and $Z = r(s)\sin(\theta(s))$, the solid line shows $r(s)$, the dashed line shows $\theta(s)$ and the dotted line shows $Y(s)$.

5. Other asymptotic scenarios for small Rb

When $Fr \ll Rb$ as $Rb \to 0$ then the equations become dominated by gravity, as can be seen from the equation for u_0 in (1.1), and rotation no longer appears at leading-order in the equation for the speed of the jet. Equation (1.5) shows that $\kappa_2 = O\left(Fr^2/Rb^3\right)$ for $Fr \ll Rb$ as $Rb \to 0$ at $s = 0$. So for $Fr = O\left(Rb^{3/2}\right)$ then $\kappa_2 = O(1)$ at $s = 0$ for $Rb \to 0$. For $Fr \ll Rb^{3/2}$ then $\kappa_2 \to 0$ at $s = 0$ for $Rb \to$

0. Therefore, these situations are not examined in this paper since κ_2 is not asymptotically large in this situation for $Fr \leqslant O\left(Rb^{3/2}\right)$. Physically this scenario is associated with gravity dominating over rotation.

Also, when $Fr = O\left(Rb^{-1/2}\right)$ then $\kappa_2 = O(1)$ at $\bar{s} = 0$ from (1.5). For $Fr \gg Rb^{-1/2}$ then $\kappa_2 \to 0$ at $s = 0$ as $Rb \to 0$ from (1.5). Again, these situations are not examined in this paper since κ_2 does not become asymptotically large in this situation for $Fr \geqslant O\left(Rb^{-1/2}\right)$. Physically this scenario is associated with gravity being a weak influence on the jet.

6. Discussion

Note that in sections 2, 3 and 4, the torsion κ_2 is only asymptotically large in the inner region, and the torsion is small or $O(1)$ throughout the outer region.

Table 1 shows a summary of each of the three asymptotic calculations carried out in sections 2, 3 and 4 for $Rb \to 0$. The first column gives the scaling of Fr in each calculation from sections 2, 3 and 4 respectively. The second column shows the scaling of the torsion κ_2 at the orifice at $s = 0$ from (1.5) in each case. The third, fourth and fifth columns give the asymptotic size of κ_2 using the far-field of the inner region in each case when $s = O\left(Rb^{3/2}\right)$, when $s = O(Rb)$ and when $s = O\left(\sqrt{Rb}\right)$ (so that $\bar{s} = O\left(Rb^{-1/2}\right)$, $\bar{s} = O\left(Rb^{-1}\right)$ and $\bar{s} = O\left(Rb^{-3/2}\right)$ respectively) which correspond to early, mid and far points in the inner region far-field. The sixth column gives the asymptotic size of κ_2 in the outer region when $s = O(1)$ in each asymptotic calculation. Finally, the seventh column gives the behaviour of κ_2 as $s \to \infty$ at the far-field of the outer region.

It can be seen that κ_2 is only large in a narrow region for $0 \leqslant s < O\left(Rb^{1/2}\right)$. Once $s = O\left(Rb^{1/2}\right)$ then the torsion is no longer large in any of the three scenarios. This means that the torsion can only be crucial to the flow in a narrow region close to the orifice for $Rb \ll 1$.

Also note that the table shows that asymptotically large values of the torsion persist longest for $Fr = O(Rb)$, though it is still only $O(1)$ when $s = O\left(Rb^{1/2}\right)$ and thus no longer asymptotically large. In fact, for the first two asymptotic calculations, for $Fr = O(1)$ and $Fr = O\left(Rb^{1/2}\right)$, then the torsion has decayed so rapidly that it is much less than $O(1)$ in the outer region.

The most extreme region for large torsion is when $Fr = O\left(Rb^{1/2}\right)$ where $\kappa_2 = O\left(Rb^{-2}\right)$ at $s = 0$. However, the torsion quickly decays to $O(Rb)$ in the outer region in this scenario.

Decent *et al.* (2018) showed that the slender jet model may break-down if the torsion is asymptotically large, and in particular argued that this may occur if $\kappa_2 = O\left(\varepsilon^{-1}\right)$. Consider this first in the context of the scenario discussed in section 2. If $Rb = O(\varepsilon)$ and $Fr = O(1)$ then $\kappa_2 = O\left(\varepsilon^{-1}\right)$ at $s = 0$ from (1.5). Therefore, $|\kappa_2| \ll O\left(\varepsilon^{-1}\right)$ at $s = 0$ so long as $\varepsilon \ll Rb$ when $Fr = O(1)$. However, it is instructive to consider what happens as $Rb \to \varepsilon$ for $Fr = O(1)$. When $Rb = O(\varepsilon)$ for $Fr = O(1)$ then the part of the inner region where the torsion is $O\left(\varepsilon^{-1}\right)$ is at most from the orifice at $s = 0$ until $s = O\left(Rb^{3/2}\right) = O\left(\varepsilon^{3/2}\right)$ from Table 1 (where the torsion has become $O(1)$), where $\varepsilon \to 0$. It would appear to be in this small region for $Rb = O(\varepsilon)$ and $Fr = O(1)$ where the method developed by Wallwork *et al.* (2002) and Decent *et al.* (2002) might become invalid. (When the method breaks down, then the torsion may become sufficiently large to appear in the modified leading-order jet equations.)

The arguments made in the previous paragraph for section 2 can now be repeated for section 3. When $Rb \ll 1$ and $Fr = O\left(Rb^{1/2}\right)$, then $\kappa_2 = O\left(\varepsilon^{-1}\right)$ at $s = 0$ if $Rb = O\left(\varepsilon^{1/2}\right)$ and $Fr = O\left(\varepsilon^{1/4}\right)$ from (1.5). Therefore, $|\kappa_2| \ll O\left(\varepsilon^{-1}\right)$ at $s = 0$ so long as $\varepsilon^{1/2} \ll Rb$. However, as $Rb \to \varepsilon^{1/2}$ for $Fr = O\left(Rb^{1/2}\right)$ in section 3, then the length of the inner region where the torsion may be $O\left(\varepsilon^{-1}\right)$ would be at most

Table 1. Comparison of the asymptotic size of the torsion κ_2 for the three asymptotic calculations carried out in this paper, showing $Fr = O(1)$, $Fr = O\left(Rb^{1/2}\right)$ and $Fr = O(Rb)$ for $Rb \to 0$ (from sections 2, 3 and 4 respectively), for different asymptotic sizes of the arclength s. For each asymptotic size of Fr, the table shows the asymptotic size of the torsion κ_2 at the orifice (where $s = 0$), at three (early, mid and far) points in the far-field of the inner region, in the outer region (when $s = O(1)$) and at the far-field of the outer region (where $s \to \infty$).

1st column: Size of Fr	2nd column: Size of κ_2 at orifice where $s = 0$	3rd column: Size of κ_2 at an early point of far-field in inner region where $s = O\left(Rb^{3/2}\right)$	4th column: Size of κ_2 at a mid-point of far-field in inner region where $s = O(Rb)$
$Fr = O(1)$	$\kappa_2 = O\left(Rb^{-1}\right)$	$\kappa_2 = O(1)$	$\kappa_2 = O(Rb)$
$Fr = O\left(Rb^{1/2}\right)$	$\kappa_2 = O\left(Rb^{-2}\right)$	$\kappa_2 = O\left(Rb^{-1}\right)$	$\kappa_2 = O(1)$
$Fr = O(Rb)$	$\kappa_2 = O\left(Rb^{-1}\right)$	$\kappa_2 = O\left(Rb^{-1}\right)$	$\kappa_2 = O\left(Rb^{-1}\right)$

5th column: Size of Fr	6th column: Size of κ_2 at a far point of far-field in inner region where $s = O\left(Rb^{1/2}\right)$	7th column: Size of κ_2 in outer region where $s = O(1)$	8th column: Size of κ_2 in far-field of outer region where $s \to \infty$
$Fr = O(1)$	$\kappa_2 = O\left(Rb^2\right)$	$\kappa_2 = O\left(Rb^2\right)$	$\kappa_2 = O\left(s^{-1/2}Rb^2\right)$
$Fr = O\left(Rb^{1/2}\right)$	$\kappa_2 = O(Rb)$	$\kappa_2 = O(Rb)$	$\kappa_2 = O\left(s^{-1/2}Rb\right)$
$Fr = O(Rb)$	$\kappa_2 = O(1)$	$\kappa_2 = O(1)$	$\kappa_2 = O\left(s^{-1/2}\right)$

from $s = 0$ at the orifice until $s = O\left(Rb^{3/2}\right) = O\left(\varepsilon^{3/4}\right)$ using Table 1 (where the torsion has become an order of magnitude smaller in Rb) where $\varepsilon \to 0$, and it would appear to only be in this small region for $Rb = O\left(\varepsilon^{1/2}\right)$ and $Fr = O\left(Rb^{1/2}\right)$ where the method developed by Wallwork *et al.* (2002) and Decent *et al.* (2002) might become invalid.

The above can also be considered for section 4. When $Rb \ll 1$ and $Fr = O(Rb)$, then $\kappa_2 = O\left(\varepsilon^{-1}\right)$ at $s = 0$ if $Rb = O(\varepsilon)$ and $Fr = O(\varepsilon)$ from (1.5). Therefore, $|\kappa_2| \ll O\left(\varepsilon^{-1}\right)$ at $s = 0$ so long as $\varepsilon \ll Rb$. As $Rb \to \varepsilon$ for $Fr = O(Rb)$ in section 4, then the length of the inner region where the torsion may be $O\left(\varepsilon^{-1}\right)$ would be at most from the orifice at $s = 0$ until $s = O\left(Rb^{1/2}\right) = O\left(\varepsilon^{1/2}\right)$ using Table 1 (where the torsion has become $O(1)$) for $\varepsilon \to 0$, and it would appear to be only be in this region for $Rb = O(\varepsilon)$ and $Fr = O(Rb)$ where the method developed by Wallwork *et al.* (2002) and Decent *et al.* (2002) may become invalid.

Thus asymptotically large torsion such that $\kappa_2 = O\left(\varepsilon^{-1}\right)$ occurs only in a narrow inner region close to the orifice, and this region is asymptotically small as $\varepsilon \to 0$. Over this narrow region the torsion quickly becomes small or $O(1)$ as the flow emerges out of this narrow region. (The jet is not asymptotically slender when $\kappa_2 = O\left(\varepsilon^{-1}\right)$ since s would have to be rescaled with ε in a narrow orifice based region. From the underlying Euler equations the appropriate scaling in such a region would appear to be $s = O(\varepsilon)$.)

Figure 3 shows the torsion determined from a numerical solution to (1.1) when $Rb = O(1)$. In comparison, Figure 11 shows the torsion κ_2, plotted against arclength s, determined from a numerical solution of equations (1.1) when Rb is fairly small, namely for $Rb = 0.1$. (Though ε is typically much smaller than 0.1.) Figure 11 shows three curves, for $Fr = 1$ (corresponding to section 2), for $Fr = 0.3$ (corresponding to section 3), and for $Fr = 0.1$ (corresponding to section 4). The Weber number $We = 10$ for all three curves. It can be seen that there are steep gradients close to $s = 0$ and that these numerical solutions decay to zero in each case, as in sections 2, 3 and 4. As Rb decreases further below 0.1, then the asymptotics show that $|\kappa_2|$ will become larger at $s = 0$ but will also decay more rapidly to zero as s increases.

Other physical effects neglected in previous studies are likely to become more important for these high rotation rates. The shape of the orifice and flow within the orifice may become more important in a narrow region close to the orifice. Also the flow of air caused by the rotating container will be expected to interact with the jet at high rotation rates, due to the increased influence of air resistance caused by ambient pressure and frictional forces. Fenn & Middleman (1969) define a criterion for the influence of air resistance upon Newtonian jets in quiescent air when a critical Weber number (based upon the air density rather than the liquid density) exceeds a value of 5.3. Whilst this is an order of magnitude larger than the values used in most simulations and physical experiments, the additional air flow caused by the rotating container nevertheless will have a significant impact on the jet trajectory and break-up in practice at high rotation rates. This has not been included in the model described here.

In summary, in this paper the most extreme situations for the torsion have been examined for which $Rb \ll 1$, and in these situations the torsion may only be important in an asymptotically narrow region close to the orifice. If the torsion does not become sufficiently large at the orifice to cause the slender model to become invalid, then the asymptotic method developed by Wallwork *et al.* (2002) and Decent *et al.* (2002) is valid everywhere on the jet. If the torsion is sufficiently asymptotically large at the orifice (and Decent *et al.* (2018) argued that the torsion would need to be $O\left(\varepsilon^{-1}\right)$), then the method developed by Wallwork *et al.* (2002) and Decent *et al.* (2002) may break-down in a narrow asymptotic region that scales with ε close to the orifice where $\varepsilon \to 0$. This means that it has been shown here that asymptotically large torsion can only be maintained on the jet for an asymptotically short distance.

Once away from this narrow inner region then the jet will be able to be described by the outer region equations found in this paper in sections 2, 3 and 4, which are simplified versions of the trajectory equations found previously by Wallwork *et al.* (2002) and Decent *et al.* (2002). Also initial conditions can be determined for these outer region equations. It is in this outer region where $s = O(1)$ where the jet dynamics cause travelling waves to propagate down the jet and cause it to rupture as described by Wallwork *et al.* (2002), Decent *et al.* (2002) and subsequent papers (e.g. Parau *et al.* 2006, 2007 and Uddin *et al.* 2006, 2008).

Therefore, the method of Wallwork *et al.* (2002) and Decent *et al.* (2002) can be used to describe the jet dynamics even when Rb is asymptotically small and even when the torsion $\kappa_2 = O\left(\varepsilon^{-1}\right)$ at the orifice.

REFERENCES

W. ARNE, N. MARHEINEKE, A. MEISTER & R. WEGENER (2010) Numerical analysis of Cosserat rod and string models for viscous jets in rotational spinning processes. *Math. Mod. Meth. Appl. Sci.*, **20**, 1941-1965.

S. P. DECENT, A. C. KING & I. M. WALLWORK (2002) Free jets spun from a prilling tower. *J. Eng. Math*, **42**, 265-282.

S.P. DECENT, E. I. PĂRĂU, M. J. H. SIMMONS & J. UDDIN (2018) On mathematical approaches to modelling

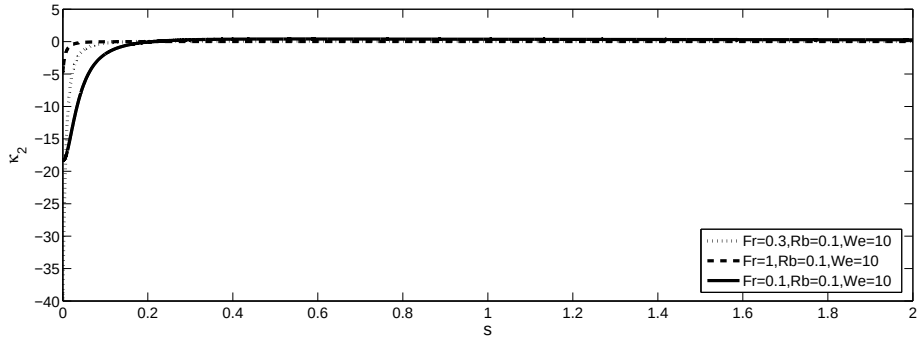

FIG. 11. The torsion κ_2 plotted against the arclength s for $Rb = 0.1$ and $We = 10$. Three curves are shown, for $Fr = 1$ (dashed line), $Fr = 0.3$ (dotted line) and $Fr = 0.1$ (solid line).

slender liquid jets with a curved trajectory. *J. Fluid Mech.*, **844**, 905-916.

R.W. FENN, & S. MIDDLEMAN (1969) Newtonian jet stability: the role of air resistance. *AIChE J.*, **15**, 3, 379-382.

S. GRAMLICH & M. PIESCHE (2012) Numerical and experimental investigations on the breakup of particle laden liquid jets in the centrifugal field. *Chemical Engineering Science*, **84**, 408-416.

V. L. HAWKINS, C. J. GURNEY, S. P. DECENT, M. J. H. SIMMONS & J. UDDIN (2010) Unstable waves on a curved non-Newtonian liquid jet. *J. Phys. A: Math. Theor.*, **43**, 055501.

J. B. KELLER & J. GEER (1973) Flows of thin streams with free boundaries. *J. Fluid Mech.*, **59**, 417 - 432.

N. MARHEINEKE, B. LILJEGREN-SAILER, M. LORENZ & R. WEGENER (2016) Asymptotics and numerics for the upper-convected maxwell model describing transient curved viscoelastic jets. MATH. MODELS METH. APPL. SCI., **26**, 569 - 600.

N. MARHEINEKE & R. WEGENER (2009) Asymptotic model for the dynamics of curved viscous figres with surface tension. J. FLUID MECH., **622**, 345 - 369.

C.-L. NG, R. SANKARAKRISHNAN & K.A. SALLAM (2008) Bag breakup of nonturbulent liquid jets in crossflow. *Int. J. Multiphase Flow*, **34**, 241-259.

S. NOROOZI, H. ALAMDARI, W. ARNE, R. G. LARSON & S. M. TAGHAVI (2017) Regularized string model for nanofibre formation in centrifugal spinning methods. *J. Fluid. Mech.*, **822**, 202-234.

S. PANDA, N. MARHEINEKE & R. WEGENER (2008) Systematic derivation of an asymptotic model for the dynamics of curved viscous fibres. *Math. Meth. Appl. Sci.*, **31**, 1153 - 1173.

E. I. PĂRĂU, S. P. DECENT, A. C. KING, M. J. H. SIMMONS & D. WONG (2006) Nonlinear travelling waves on a spiralling liquid jet. *Wave Motion*, **43**, 599-618.

E. I. PĂRĂU, S. P. DECENT, M. J. H. SIMMONS, D. WONG & A. C. KING (2007) Nonlinear viscous liquid jets from a rotating orifice. *J. Eng. Math.*, **57**, 159-179.

L. PARTRIDGE, D. C. Y. WONG, M. J. H. SIMMONS, E. I. PĂRĂU & S. P. DECENT (2005) Experimental and theoretical description of the break-up of curved liquid jets in the prilling process. *Chem. Eng. Res. Des.*,

83(A11), 1267-1275.

D. N. RIAHI (2017) Modeling and computation of nonlinear rotating polymeric jets during forcespinning process. *International Journal of Non-Linear Mechanics*, **92**, 1-7.

N. M. RIBE (2004) Coiling of viscous jets. *Proc. R. Soc. Lond. A*, **460**, 3223 - 3239.

N. M. RIBE, M. HABIBI & D. BONN (2006) Stability of liquid rope coiling. *Physics of Fluids*, **18**, 084102.

Y. D. SHIKHMURZAEV & G. M. SISOEV (2017) Spiralling liquid jets: verifiable mathematical framework, trajectories and peristaltic waves. *J. Fluid Mech*, **819**, 352-400.

J. UDDIN, S. P. DECENT & M. J. H. SIMMONS (2006) The instability of shear thinning and shear thickening spiralling liquid jets: linear theory. *ASME J. Fluids Eng.*, **128**, 968-975.

J. UDDIN, S. P. DECENT & M. J. H. SIMMONS (2008) The effect of surfactants on the instability of a rotating liquid jet. *Fluid Dynamics Research*, **40**, 827-851.

I. M. WALLWORK, S. P. DECENT, A. C. KING & R. M. S. M. SCHULKES (2002) The trajectory and stability of a spiralling liquid jet. Part 1. Inviscid theory. *J. Fluid Mech*, **459**, 43-65.

D. WONG, M. J. H. SIMMONS, S. P. DECENT, E. I. PĂRĂU & A. C. KING (2004) Break-up dynamics and drop size distributions created from spiralling liquid jets. *Int. J. Multi-Phase flow*, **30**, 499-520.